15

Development of a laser-plasma spark targets echelon for an EUV nanolithography light source

© T.V. Chernoiziumskaya,[1] V.Y. Sergeev,[1] V.V. Kontorin,[1] D.E. Beliaevskii,[2] M.K. Buts,[1] V.G. Kapralov,[1] P.A. Karaseov,[1] D.D. Korobko,[1] M.A. Tsaregorodtsev,[1] I.A. Sharov[1]

[1]Peter the Great Saint-Petersburg Polytechnic University,
195251 St. Petersburg, Russia
[2] „TechnoSystemTrade LLC“,
197342 St. Petersburg, Russia
e-mail: t.chernoizyumskaya@spbstu.ru

Received August 9, 2025
Revised November 14, 2025
Accepted November 14, 2025

The test-bed setup for producing echelon of laser-plasma spark targets for an EUV nanolithography light source was designed and commissioned. The development of Plateau-Rayleigh instability in a liquid argon jet has been experimentally observed and recorded using high-speed video. Targets in the echelon have average diameter of 0.2 mm and a spatial period of 0.5 mm. These parameters are promising to be utilized in a EUV light source for nanolithography.

Keywords: target, echelon, EUVL, laser-plasma spark, nanolithography, xenon, argon.

DOI: 10.61011/TP.2026.04.63280.206-25

Introduction

Implementation of a nanolithography process in modern production of nanometer-resolution chips requires power sources emitting at about 10 nm [1]. ASML (the Netherlands) is the only company in the world that manufactures extreme ultraviolet lithography machines. Source of extreme ultraviolet (EUV) light in such machine is plasma spark formed when laser radiation interacts with tin atoms (radiation at the wavelength of 13.5 nm). A general concept of the industrial lithography machine that involves tin use was adopted in 2008–2009 [2]. This choice is not optimal, since the use of metal requires solving the problem of tin vapor deposition on the elements of the optical system that forms the working flux of photons. Presently, this problem is solved by means of a set of special equipment and regular maintenance.

An alternative material that could be used as a source of radiation for the nanoscale lithography is xenon [1]. When interacting with laser radiation, xenon atoms form plasma containing, in particular, multiply ionized xenon ions ($Z = 9-11$). These ions can emit photons at 11.2 nm. The conversion efficiency (CE) of pumping power to working radiation when using xenon is 2–3 times less than when using tin [3]. Such efficiency reduction takes place when a mirror made of the same material (Mo/Si) as a mirror for Sn plasma is used for Xe plasma radiation collection. However, quite recently Be-based interference mirrors having the maximum of reflection at 11.2 nm have been designed [4]. Application of these mirrors will make it possible to obtain higher CE values of the Xe-based EUV light sources. Xenon use completely excludes contamination of the optical elements by a deposit of a working material. At the same time, an important problem is to design a technology to deliver xenon to an area of its excitation by laser radiation. At early stages of nanolithography development, xenon injection as a gas jet flowing out of a pressurized vessel through a small-diameter channel (capillary) has been used. For example, an improved two-flow coaxial capillary is described in [5], and its later application is presented in [6]. Another technique is formation of a supersonic low-temperature xenon jet with small radial expansion, as described in [7,8]. It is known that CE depends on a density of the gas jet in the excitation volume. The density rapidly drops with the distance from the capillary outlet. An attempt to move the excitation area closer to the capillary outlet results in sputtering of a capillary walls and its destruction [3], since a considerable amount of energy is released when a laser spark is ignited. Efficiency of laser-plasma radiation generation is noticeably reduced if the excitation volume is located at a safe distance from the capillary output. It necessitates designing a method of jet production, in which the material is in a condensed state with the significantly higher density. Thus, it is necessary to design a technology to deliver xenon in the condensed state into a region that is far enough from a capillary nozzle, for subsequent ignition of the laser spark. Presently, systems for supplying jets of a various composition into the sources of laser-plasma radiation are actively developed [9]. It seems that for the EUV light source for the nanolithographer it is preferable to use echelon of targets, rather than a solid jet part, since it can solve a problem of pressure growth in a first-mirror area due to debris formed when the continuous jets interacts with laser radiation [3]. There

Table 1. Triple point and rheological characteristics of argon and xenon

Parameter	Argon	Xenon
Triple point pressure, kPa	69	82
Triple point temperature (T3), K	83.8	161.4
Density at the temperature of about T3, t/m^3	1.4	2.9
Viscosity at the temperature of about T3, Pa·s	$2.6 \cdot 10^{-4}$	$5 \cdot 10^{-4}$
Coefficient of surface tension at the temperature of about T3, N/m	$1.3 \cdot 10^{-2}$	$1.8 \cdot 10^{-2}$

have been previously attempts to create systems to inject liquified noble gas jet of a small diameter $10-20\,\mu$m [3] and studying CE of such radiation sources. But low heat capacity and thermal conductivity of such a thin capillary make it difficult to provide a stable temperature mode required for maintaining an injected material in the liquid state.

The present study is aimed to experimentally investigate the process of injection of the liquified argon jet of the diameter of about $100\,\mu$m into a closed chamber with controlled pressure of the injected substance vapor. It is profitable to utilize argon at the early stage of technological process development, since it is a more affordable and cheaper material. A transition to xenon shall not raise technological problems, as the rheological characteristics of argon and xenon are close as specified in Table 1. The higher temperature of the xenon triple point as compared to argon will facilitate cooling process.

In the present study parameters of the gas and heat system for production of the stable liquified argon jet are investigated. Specific features of a progress of Plateau-Rayleigh instability that result in formation of the argon droplets echelon are described.

1. Description of the experimental setup

A diagram of the designed experimental setup is shown in Fig. 1. Argon under pressure is supplied into the trunk line *1* from the cylinder *2* through the reducer *3*. Pressure in the argon trunk line is controlled by an output pressure gauge of the reducer. Possibility to evacuate the argon trunk line via the bypass line *4* is realized. The cryostat chamber *5* is evacuated by the turbomolecular pump *6* and the primary vacuum pump *7*. Pressure in the cryostat chamber is measured by the vacuum gauge *8*. The liquid nitrogen filled cryostat *9* is attached to the cryostat chamber *5* by the heat-insulating flange *10*. The argon trunk line is connected to the chamber *5* via the flange *11* by a mushroom-like

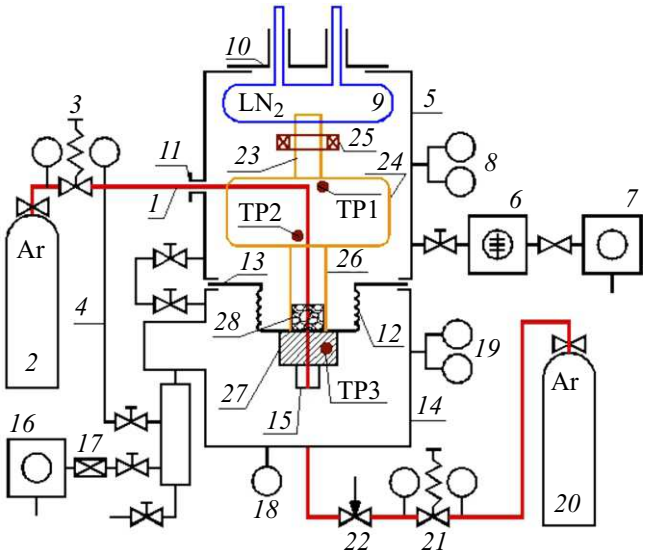

Figure 1. Diagram of the experimental setup for production of the liquid argon jet. (Explanations are given in the text.)

sealing. The bellows thermovacuum barrier *12* is installed by means of a flange to a hole of the partition wall *13* that separates the cryostat chamber and the jet formation chamber *14* (FC). The argon trunk line *1* is connected to the FC via the capillary *15*. The FC is evacuated by the primary vacuum pump *16*. Evacuation rate can be adjusted by the throttle valve *17*. FC pressure is measured by the vacuum-pressure gauge *18* (measurement of the pressure at around the Ar triple point) and the vacuum gauge *19* (average and low pressure measurement). Possibility to inject argon into the FC from the cylinder *20* via the reducer *21* and the leak *22* is additionally designed.

The cryostat *9* is brought into a thermal contact with the heat-exchanger liquefier *24* by the cold finger *23* t.

The liquefier is a bulk sealed copper piece in which a well developed system of channels is made. It is tightly bounded to the cryostat cold finger immersed in the liquid nitrogen. The entire system is located in the evacuated chamber in order exclude unwanted heat gains.

An operating principle is based on surface condensation of pressurized gaseous argon in the heat-exchanger channels that are cooled to the temperature below the point of the phase transition. An outlet hole (needle–throttle) makes it possible to create the operating pressure in a condensation area that is required for effective heat transfer and increase the condensation temperature. The needle is cooled both at the mounting contact as well as by adiabatic pressure drop (the Joule-Thomson effect). Thus, we achieve a combined process of argon cooling, condensation in the heat exchanger and additional cooling due to the throttle effect.

Hydraulic resistance of the heat-exchanger channel is negligible as compared to hydraulic resistance of the capillary, as the cross-section of the heat exchanger channel

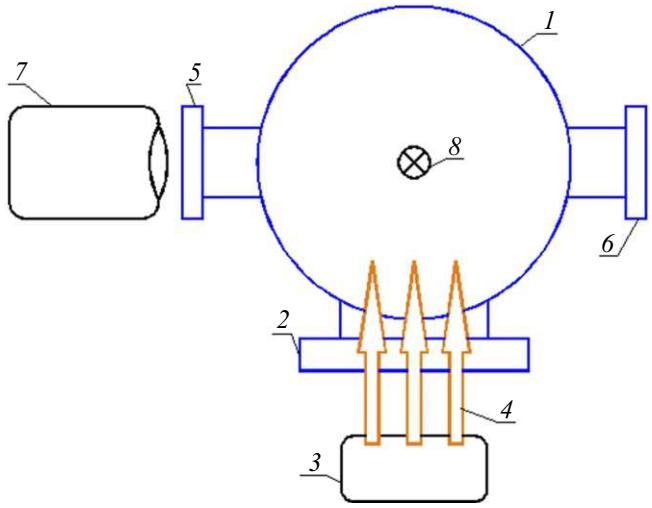

Figure 2. Diagram of video recording of formation of the jet and the argon droplets echelon. Plan view: *1* — FC, *2* — the illumination window, *3* — the illuminating lamp, *4* — the direction of light, *5* — the window for high-speed video recording, *6* — the background window (also used for photo recording with low time resolution), *7* — the high-speed video camera, *8* — the jet.

by six orders of magnitude exceeds the cross-section of the capillary, through which the liquid is injected.

The compensating heater *25* is designed to control the temperature of the heat-exchanger liquefier. Liquid argon is supplied via the tube *26* from the outlet of the heat exchanger *24* into the capillary *15* fixed in the cartridge *27*. A 32G TW-caliber needle of the length of 23 mm was used as a capillary to inject liquid argon. A needle thickness is 235 μm and inner diameter of the needle is 104 μm.

The heat exchanger temperature is controlled by the thermal sensor TP1 near the argon trunk line inlet and the thermal sensor TP2 near the argon trunk line outlet. The temperature was measured by resistive thermal sensor HEL-705 in a resistance measurement mode. A measurement error is 1 K.

The outlet of the liquefier *26* was connected to the capillary *15* using a standard fitting Hy-Lok CWC-8M-4P and a specially developed cartridge *27* with an indium sealing. The thermal sensor TP3 (resistive thermal sensor HEL-705) was integrated into the cartridge using home-made technology.

In order to filter out solid-state impurities from liquid argon at the capillary inlet, a piece *28* of an analytical filter FPP-15 was used according to a recommendation specified in [10].

The bellows manufactured according to GOST 22388-90 exec.1 28-8-0.16 was included into a dedicated assembly and used as the thermo-vacuum barrier.

A diagram of photo- and video-recording is shown in Fig. 2. High-speed video recording was performed by monochrome video camera Phantom Miro M110 with a pixel size of 20 μm and a dynamic range of 12 bit. A macrolens with a focal distance of 100 mm and an F-number of f/2.8 was used. The argon jet was shot at a frame repetition rate of 1600 Hz, which corresponds to a frame period of 625 μs. Exposure was 2 μs. Paths the jet and the droplets run during the exposure time were obviously much smaller than their sizes. Duration of one video record at the above settings is about 1.3 s.

Jet was lighted by a light-emitting diode lamp that creates illumination of $2 \cdot 10^5\, lx$ with high stability. The jet and the point where the echelon of droplets starts are located in front of the background of the optical window at the side opposite to the video-recording window, thereby making it possible to have low projector background illumination.

2. Experimental results and discussion

The initial stage of the experiment included designing of technique of obtaining the stable liquid argon jet. The argon liquid state can be obtained above the triple point temperature $T_{\mathrm{Ar},triple} = 83.8$ K when the pressures exceed the triple point pressure $P_{\mathrm{Ar},triple} = 68.9$ kPa. Since it is difficult to control the temperature and pressure directly in the area of formation of the liquid phase, we have designed a procedure of obtaining the required values based on results of measurement of the sensors available.

Prior to the start of the experiment, the cryostat chamber volume was evacuated to pressure of $1.3 \cdot 10^{-3}$ Pa. The FC volume was evacuated to pressure of $2.6 \cdot 10^{-1}$ Pa with simultaneous evacuation of the argon trunk line. After specified vacuum was achieved, the cryostat was filled with liquid nitrogen. The time to working mode was 45 min. During cooling the temperature was measured by the thermal sensors TP1 an TP2. Due to specific features of the setup, the temperature of the cartridge and the capillary was stabilized at 140 K at this stage. In order to cool the cartridge with the capillary and the outlet of the heat exchanger, which takes off liquified argon, when the temperature of 86 K is recorded at the TP2 thermal sensor, argon was admitted into the supply line under pressure $P_{\mathrm{Ar}} = 2 \cdot 10^5$ Pa. The capillary was cooled at constant FC pressure set at 80 Pa.

Some time after supply of argon into the heat exchanger, when the readings of the TP3 thermal sensor came below 100 K, with FC pressure of 80 Pa pulsating gas-vapor mixture appeared from the capillary in the form of a wide spray partly transiting to the solid phase. In cases pressure in the formation chamber was as low as 80 Pa, for 10 min and more while when achieving the TP3 reading below 100 K, argon turned to solid state in the heat exchanger, flow from the capillary has broken and the system stopped reacting to variation of pressure in the formation chamber. The working mode returned by heating it up with the compensating heater at power of 40 W. The warm-up time was 20 min.

In order to avoid this effect and to obtain stable jet generation, the FC was shifted to the working mode with pressure of 80 kPa when the readings of the TP3 thermal

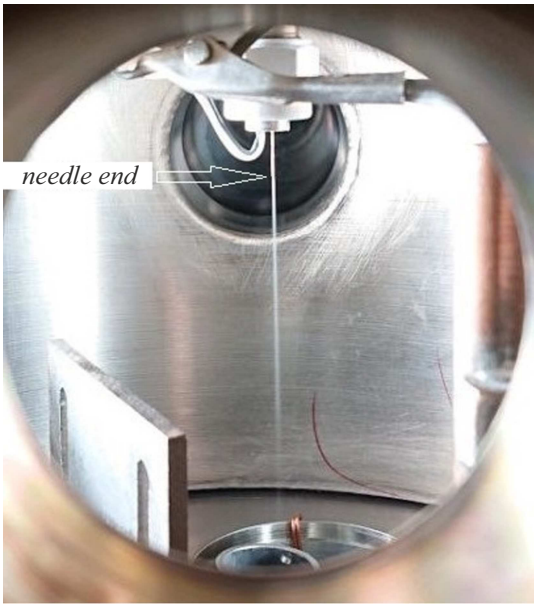

Figure 3. Liquid argon jet shot by means of the photo camera of low time resolution.

sensor were below 90 K. This pressure is selected basing on a technical capability to maintain minimum stable pressure above the value of $P_{\mathrm{Ar},triple}$ by adjusting a cross section of the pumping line by means of the throttle valve *17* with control by the pressure and vacuum gauge *18*. Argon could also be admitted into the FC from the cylinder *20* via the reducer *21* and the leak *22*. Transfer of the FC into the working mode was followed by an abrupt transition to output of liquid argon from the capillary with jet pulsations going over to a spray. When pressure in the argon trunk line increases to $4 \cdot 10^5$ Pa, the jet was stabilized for 1 min and then remained stable for the entire period of video recording (> 30 min).

It was shown by measuring the temperature of the needle cartridge by the TP3 thermal sensor that when a liquid flow through the capillary occurs, the cartridge temperature decreases by the value of 12 K for 10 s. It indicates significant influence of the liquid flow on thermal balance of the cartridge and the capillary.

The Fig. 3 shows a photo of the liquid argon jet that is obtained with exposure of 33 ms at the following parameters of injection: pressure in the argon trunk line is $4 \cdot 10^5$ Pa, FC pressure is 80 kPa, the temperature at the needle cartridge is 88 K. It can be seen that the stable argon jet of the length $\cong 100$ mm is formed.

Fig. 4 shows instantaneous photos of the jet, which are shot with the time of exposure of $2\,\mu$s. We observe a clear picture of disintegration of the continuous jet into the echelon of separate droplets. It is disintegrated at a certain distance L_{jet} from a capillary end, from which the jet flows, due to development of the Plateau-Rayleigh instability. The value of the said distance increases with an increase of pressure in the argon trunk line.

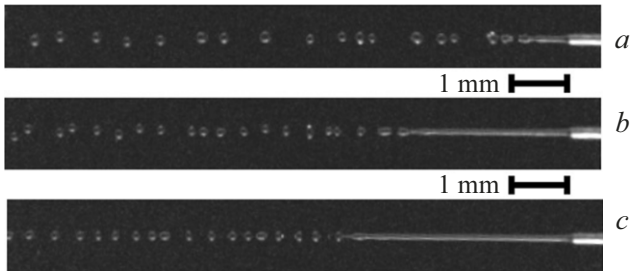

Figure 4. Formation of the droplets echelon from the argon jet due to development of the Plateau-Rayleigh instability at the various pressures in the argon trunk line: *a* — $4 \cdot 10^5$ Pa, *b* — $5 \cdot 10^5$ Pa, *c* — $6 \cdot 10^5$ Pa. Shot by means of the high-rate video camera.

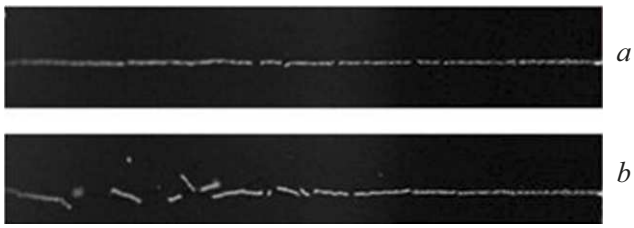

Figure 5. Collapse of the argon solid-phase jet at the reduced FC pressure: *a* — $6 \cdot 10^4$ Pa, *b* — $4 \cdot 10^4$ Pa. Shot by means of the high-rate video camera.

At pressures 40–70 kPa in the FC and $4 \cdot 10^5$ Pa in the argon supply line the liquid transited into the solid phase directly at the needle outlet with formation of a long thread of solid argon, which started breaking apart at the distance about 20–30 mm from the needle end. The photos of this process are shown in Fig. 5.

With further reduction of FC pressure to 20 kPa and below argon started exiting the needle in the solid phase as thin curling hairs of the length about 20–50 mm.

The photos shown in Fig. 4 make it possible to directly measure geometrical characteristics of the jet and the echelon, using the known external capillary diameter of $235\,\mu$m.

In all the cases, the observed values of the diameter of the droplets being formed are approximately two diameters of the jet. The distance between the droplets L_{dr}, the droplets echelon period and the droplets diameter D_{dr} are unstable. For the data shown in Fig. 4, *a*–*c*, correspondingly, the observed average values $\langle L_{dr} \rangle = 480$, 340, 320 and $\langle D_{dr} \rangle = 240$, 220, 200 μm.

The classic model of development of the Plateau-Rayleigh determines the geometrical characteristics of the droplets echelon being formed, as follows [11]:

$$L = \frac{\pi}{0.7}\, d \cong 4.5d, \tag{1}$$

$$D = (6.75)^{1/3} d \cong 1.9d. \tag{2}$$

Table 2. Results of statistical processing of high-speed video recording of argon droplet echelon: dL_{fr}, dL_{jet} is a standard deviation of the lengths L_{fr}, L_{jet}

P_{Ar}	L_{fr}	dL_{fr}	L_{jet}	dL_{jet}	V_{jet}
kPa	mm	mm	mm	mm	m/s
400	0.26	0.05	1.04	0.21	0.42
500	0.38	0.05	3.09	0.16	0.61
600	0.41	0.01	4.49	0.21	0.66

Here, d is a jet diameter (it is assumed to be equal to the capillary's internal diameter of $104\,\mu$m), L is a distance between the droplets in the echelon, D is a diameter of the droplet. The expressions (1) and (2) are obtained by assuming that there are not mechanical oscillations of the capillary, from which the jet exits. It is clear that the observed average values $\langle L_{dr}\rangle$ and $\langle D_{dr}\rangle$ quite well correspond to estimates $L \cong 470\,\mu$m and $D \cong 200\,\mu$m, which are made by means of the expressions (1) and (2). Observed instability of the values of L_{dr} and D_{dr} can be due to influence of vibrations of the experimental bench.

In many cases, individual droplets could be identified frame by frame based on their size and shape. It makes it possible to determine an echelon speed by two frames that are close in time. The geometrical characteristics and the echelon speed were statistically analyzed by means of processing large arrays (2052 frames per each of the three studied pressures) of the obtained images using purposefully-designed software. The speed V_{jet} of the argon droplets echelon was assumed to be equal to the jet speed and measured as a ratio of an echelon shift L_{fr} per frame to the frame period. The processing results are shown in Table 2.

The observed spread of the measured values can be related to presence of an irregular background vibrations of the capillary perpendicular to the injection axis. It results in fluctuations of an amplitude of initial oscillations of the jet surface, thereby causing fluctuations of the time of the Plateau-Rayleigh instability development takes and hence length of the continuous part of the jet, as well as fluctuations of the speed of the jet and the echelon.

The measured values of the speed of the jet and the argon droplets echelon V_{jet} were compared to Poiseuille formula's estimates for the jet speed at the capillary axis V_0 [12]:

$$V_0 = \frac{\Delta P R^2}{4bL}, \tag{3}$$

where ΔP is a capillary pressure drop, $R = d/2 = 52\,\mu$m is an internal radius of the capillary, b is dynamic viscosity of the liquid, L is a length of the capillary. According to [10], dynamic viscosity of argon at 90 K is $2.25 \cdot 10^{-4}$ Pa·s, and at 120 K it is $1.17 \cdot 10^{-4}$ Pa·s. In our experiments, the temperature of the cartridge that holds the capillary through which liquid argon passes was measured. Technically, It is not possible to measure the temperature of liquid argon moving inside the needle, therefore, all the calculations are done for the two temperatures of liquid argon: V_{01} for 90 K (the value that is close to the cartridge temperature of TP3 $\cong$ 88 K measured during injection) and V_{02} for 120 K for estimating influence of possible heating of argon due to viscous friction in the capillary. The capillary length $L = 23$ mm is accepted to be equal to the needle length. The pressure drop across the capillary ΔP was taken as the difference between pressure of $P_{\mathrm{Ar}} = [400, 500, 600]$ kPa in the argon trunk line and FC pressure of 80 kPa. The calculation results are presented in Table 3.

Table 3. Comparison of the experimental results and the calculations of the echelon parameters.

P_{Ar}	V_{01}	V_{02}	t_{jet}	t_{R1}	t_{R2}
kPa	m/s	m/s	ms	ms	ms
400	42	80	2.5	1.7	2.4
500	55	106	5.1	1.7	2.4
600	68	131	6.8	1.7	2.4

The jet speeds V_{01} and V_{02} that are calculated by the formula (3) and given in Table 3 significantly exceed the experimentally measured ones $V_{jet} \cong 0.4{-}0.7$ m/s. It should be noted here that during the experiments the observed phase transition of argon during cooling in the heat exchanger was always observed at adequate measured values of pressure in the argon trunk line and the temperature of the heat exchanger, thereby indicating that there are not any significant pressure losses throughout the argon trunk line, including in the heat exchanger. Probably, to calculate jet acceleration in the submillimeter-diameter capillary, it is necessary to take into account influence of the filter and processes in a boundary layer of the liquid near the capillary wall [13] as well as a possible increase of hydrodynamic resistance of the capillary as a result of reduction of its effective diameter due to freeze-on of argon on its walls.

By the experimental results, the time of development of the Plateau-Rayleigh instability can be estimated as $t_{jet} = L_{jet}/V_{jet}$ and is given in Table 3. According to the Plateau-Rayleigh model, the time of development of the instability τ_R is determined as follows [11,14,15]:

$$t_R = \frac{\ln(1/x)}{0.35\sqrt{8}}\sqrt{\frac{n \cdot d^3}{s}}. \tag{4}$$

Here, d is the jet diameter, $n$is the density of liquid argon, s is surface tension of liquid argon, x is amplitude of initial disturbance of the jet surface expressed as the fraction of the jet radius. A relative amplitude of initial disturbance of the jet surface for estimates as per the Plateau-Rayleigh model can be selected by results of the previous experimental studies [14,15], which report a range

Table 4. Estimates (5) of the argon flow in the droplets echelon

P_{Ar}	V_{jet}	G_{Ar1}	G_{Ar2}
kPa	m/s	10^{19} at/s	10^{19} at/s
400	0.42	7.34	6.19
500	0.61	10.7	9.05
600	0.66	11.67	9.76

$x = 0.01 - 0.1$. Table 3 presents results of calculations of t_{R1} for 90 K and t_{R2} for 120 K with values of the density of liquid argon of $n_{\mathrm{Ar1}} = 1376\,\mathrm{kg/m^3}$, $n_{\mathrm{Ar2}} = 1160\,\mathrm{kg/m^3}$ and the surface tension of liquid argon of s $11.8 \cdot 10^{-3}$ N/m, $4.95 \cdot 10^{-3}$ N/m for the respective temperatures according to [10]. The parameter x in (4) was accepted to be 0.01. It is clear from Table 3 that the estimation of the time of the instability development made according to the Plateau-Rayleigh model t_{R1}, t_{R2} coincide with the experimental results taking into account the experimental data spread caused, as mentioned above, by irregular background vibrations of the capillary and uncertainties of the unmanageable parameter x.

An important characteristic of targets when creating the radiation source in the EUV nanolithographer is a flow of target atoms into the area of the laser-plasma spark ignition. In modern devices produced by ASML the liquid tin targets of the size $D_{\mathrm{Sn}} \cong 30\,\mu$m are supplied with a frequency $f_{\mathrm{Sn}} \cong 50\,$kHz [16]. Since the size of a caustic (focus) of a laser spot exceeds D_{Sn} and if all tin atoms take part in creating radiating plasma, it is possible to estimate a flow of tin atoms G_{Sn} as

$$G_{\mathrm{Sn}} = \frac{n_{\mathrm{Sn}} \cdot \pi \cdot D_{\mathrm{Sn}}^3}{6 \cdot M_{\mathrm{Sn}}} \cdot f_{\mathrm{Sn}} \cong 2.5 \cdot 10^{19}\,\mathrm{at/s}.$$

Here, $n_{\mathrm{Sn}} \cong 6990\,\mathrm{kg/m^3}$ is a density of melt tin, M_{Sn} is tin atomic mass.

The obtained experimental data on the speed V_{jet} and the average values of the diameter $\langle D_{dr} \rangle$ and the period $\langle L_{dr} \rangle$ of the argon droplets make it possible to estimate the flow of the target atoms leaving the capillary, as given in Table 4:

$$G_{\mathrm{Ar1,2}} = \frac{n_{\mathrm{Ar}}(T) \cdot \pi \cdot \langle D_{dr} \rangle^3}{6 \cdot M_{\mathrm{Ar}}} \cdot \frac{V_{jet}}{\langle L_{dr} \rangle}, \qquad (5)$$

where M_{Ar} is an atomic mass of argon. It has been calculated at two argon temperatures, i.e. — 90 K (G_{Ar1}) and 120 K (G_{Ar2}).

The supply frequency $V_{jet}/\langle L_{dr} \rangle = (0.6\,\mathrm{m \cdot s^{-1}})/(340\,\mu\mathrm{m}) \cong$ $\cong 1.8\,$kHz (for $P_{\mathrm{Ar}} = 500\,$kPa) is low due to low values of V_{jet}. In order to obtain the frequency of 50 kHz, the speeds $V_{jet} \cong 17\,$m/s must be achieved, which increases the values of the flow $G_{\mathrm{Ar}} \cong 3.0 \cdot 10^{21}$ at/s. Thus, with the target diameter increasing, it is necessary to use only a small portion $G_{\mathrm{Sn}}/G_{\mathrm{Ar}} \cong 0.009$ of atoms supplied into the area of the focus of the laser spot in order to achieve maximum efficiency of the radiation source. It can be expected that in the proposed approach with increasing the target size to optimize the density, duration and the size of a plasma cloud that radiates on the target surface it will be possible to use the following parameters: energy, duration, the size of the focus of the laser spot and an angle of inclination of laser radiation with respect to a normal to the target surface. Moreover, it can be convenient to increase the size of the targets in the echelon, and hence their momentum, in terms of reduction of deviations of their trajectories, which is important for stable initiation of the plasma-laser spark. It also reduces requirements to accuracy of positioning of the focus of the laser spot on the surface of the target during its movement in a chamber of the lithographer's first mirror.

With the target size increase, the question raises how to maintain low pressure $0.1-1\,$Pa in the EUV light radiation source in order to keep its small optical thickness with simultaneous maintaining pressure in the capillary area above the $P_{\mathrm{Ar},triple}$. In order to solve this problem, the source of the targets for the industrial nanolithographer shall consist of several stages [14,17] with differential independent evacuation as proposed in [18].

Conclusion

The setup to study cryogenic argon droplet targets for the laser-plasma spark generation for the nanolithography EUV light radiation source has been developed and installed.

That setup was used to perform experimental investigation of the process of injection of the liquified argon jet into the separate chamber with a controlled pressure. The system parameters to achieve stable injection of the continuous liquid argon jet are determined. It was established that the measured jet speed is essentially smaller than that was expected. Possible reasons are pressure loss at the filter and the increase of hydrodynamic resistance of the capillary as a result of reduction of its effective diameter due to argon freezing on its walls.

The development of Plateau-Rayleigh instability in the liquified argon jet was experimentally observed and measured by high-speed video camera. The parameters of the produced echelon of argon droplets of 0.2 mm in diameter and spatial period of 0.5 mm are of interest to find the working regime of the EUV light source operation with droplet size in the millimeter range as compared with contemporary dimensions of the xenon jets and droplets $10-20\,\mu$m.

One can expect that the observed fluctuations of the diameter and the spatial period of the droplet echelon might be reduced by both the jet speed increase and applying controlled acoustic mechanical oscillations to the capillary nozzle.

Further steps in development of the technology will include experiments with xenon jet, development the system to deliver the target echelon into the region of plasma spark

ignition by laser shots and studies of efficiency of the EUV light radiation source.

Funding

The study is supported by State Atomic Energy Corporation Rosatom and the Ministry of Science and Higher Education of Russian Federation as a part of the Federal project „Fusion power technologies“ the of National Project of Technological Leadership „New Nuclear and Energy Technologies“, project No. FSEG-2025-0002 „Development of principles and systems to control and diagnose tokamak plasma by means of matter injection“.

Conflict of interest

The authors declare no conflict of interest.

References

[1] V. Bakshi (ed.). *EUV sources for lithography* (SPIE PRESS, 2006)
[2] H. Meiling, E. Boon, N. Buzing, K. Cummings, O. Frijns, J. Galloway, M. Goethals, N. Harned, B. Hultermans, R. de Jonge, B. Kessels, P. Kurz, S. Lok, M. Lowisch, J. Mallman, B. Pierson, K. Ronse, J. Ryan, E. Smitt-Weaver, M. Tittnich, C. Wagner, A. van Dijk, J. Zimmermann. Emerging Lithographic Technologies XII. SPIE, **6921**, 171 (2008)
[3] B.A.M. Hansson, H.M. Hertz. J. Phys. D: Appl. Phys., **37**, 3233 (2004). DOI: 10.1088/0022 3727/37/23/004
[4] M.V. Svechnikov, N.I. Chkhalo, S.A. Gusev, A.N. Nechay, D.E. Pariev, A.E. Pestov, V.N. Polkovnikov, D.A. Tatarskiy, N.N. Salashchenko, F. Schäfers, M.G. Sertsu, A. Sokolov, Y.A. Vainer, M.V. Zorina. Opt. Express, **26**, 33718 (2018). DOI: 10.1364/OE.26.033718
[5] H. Fiedorowicz, A. Bartnik, R. Jarocki, R. Rakowski, M. Szczurek. Appl. Phys. B, **70** (2), 305 (2000).
[6] N.I. Chkhalo, S.A. Garakhin, A.Ya. Lopatin, A.N. Nechay, A.E. Pestov, V.N. Polkovnikov, N.N. Salashchenko, N.N. Tsybin, S.Tu. Zuev. AIP Advances, **8** (10), 105003 (2018). DOI: 10.1063/1.5048288
[7] S.G. Kalmykov, P.S. Butorin, M.E. Sasin. J. Appl. Phys., **126**, 103301 (2019). DOI: 10.1063/1.5115785
[8] V.E. Guseva, A.N. Nechai, A.A. Perekalov, N.N. Salashchenko, N. Chkhalo. ZhTF, **92** (8), 1185 (2022) (in Russian). DOI: 10.21883/JTF.2022.08.52781.72-22
[9] V.E. Guseva, M.S. Mikhailenko, A.N. Nechai, A.A. Perekalov, N.N. Salashchenko, N. Chkhalo. Instrum. Experiment. Techniq., **67**, 67 (2024). DOI: 10.1134/S002044122470012X
[10] M.P. Malkov (red.). *Spravochnik po fiziko-tekhnicheskim osnovam kriogeniki* (Energoatomizdat, M., 1985) (in Russian)
[11] V.G. Levich. *Fiziko-himicheskaya gidrodinamika* (Gos. izd-vo Fizmatlit, M., 1959) (in Russian).
[12] L. Prandtl'. *Gidroaeromekhanika*. [per. so vtorogo nemetskogo izdaniya G.A. Vol'perta] (RKhD, M., Izhevsk, 2002) (in Russian).
[13] K.V. Sharp, R. Adrian, J.G. Santiago, J.I. Molho. *Liquid flows in microchannels* (CRC Press, 2005)
[14] A.V. Boukharov, M. Buscher, A.S. Gerasimov, V.D. Chernetsky, P.V. Fedorets, I.N. Maryshev, A.A. Semenov, A.F. Ginevskii. Phys. Rev. Lett., **100**, 174505 (2008). DOI: 10.1103/PhysRevLett.100.174505
[15] B.A.M. Hansson, M. Berglund, O. Hemberg, H.M. Hertz. J. Appl. Phys., **95**, 4432 (2004). DOI: 10.1063/1.1687037
[16] I. Fomenkov, D. Brandt, A. Ershov. Adv. Opt. Technol., **6**, 173 (2017). DOI: 10.1515/aot 2017-0029
[17] R.A. Costa Fraga, A. Kalinin, M. Kühnel, D.C. Hochhaus, A. Schottelius, J. Polz, M.C. Kaluza, P. Neumayer, R.E. Grisenti. Rev. Sci. Instrum., **83** (2), 025102 (2012). DOI: 10.1063/1.3681940
[18] V.Yu. Sergeev, P.A. Karaseov, T.V. Chernoizyumskaya, D.D. Korobko. *Ystroistvo dlya upravlyaemogo formirovaniya i podachi eshelona ksenonovykh mishenei v kameru istochnika zhestkogo ul'trafioletovogo izlucheniya* (Russian Patent № 224312, Izobreteniya. Utility Models June 2024, 2021), Bull. No. 13 (in Russian).

Translated by M.Shevelev